Electron Acceleration in Cavitated Channels Formed by a Petawatt Laser in Low-Density Plasma

S. P. D. Mangles,[1] B. R. Walton,[1] M. Tzoufras,[4] Z. Najmudin,[1] R. J. Clarke,[3] A. E. Dangor,[1] R. G. Evans,[1,5] S. Fritzler,[2] A. Gopal,[1] C. Hernandez-Gomez,[3] W. B. Mori,[4] W. Rozmus,[1,*] M. Tatarakis,[1] A. G. R. Thomas,[1] F. S. Tsung,[4] M. S. Wei,[1] and K. Krushelnick[1]

[1]*Blackett Laboratory, Imperial College London, SW7 2BZ, United Kingdom*
[2]*Laboratoire d'Optique Appliquée, École Nationale Supérieure des Techniques Avancées, École Polytechnique, CNRS, UMR 7639, 91761 Palaiseau, France*
[3]*Central Laser Facility, Rutherford Appleton Laboratory, Oxon, OX11 0QX, United Kingdom*
[4]*Department of Physics and Astronomy, UCLA, Los Angeles, California 90095, USA*
[5]*AWE plc, Aldermaston, Reading RG7 4PR, United Kingdom*

(Received 12 April 2004; revised manuscript received 29 March 2005; published 21 June 2005)

The spectra of energetic electrons produced by a laser interaction with underdense plasma have been measured at intensities $>3 \times 10^{20}$ W cm^{-2}. Electron energies in excess of 300 MeV have been observed. Measurements of the transmitted laser spectrum indicate that there is no correlation between the acceleration of electrons and plasma wave production. Particle-in-cell simulations show that the laser ponderomotive force produces an ion channel. The interaction of the laser field with the nonlinear focusing force of the channel leads to electron acceleration. The majority of the electrons never reach the betatron resonance but those which gain the highest energies do so. The acceleration process exhibits a strong sensitivity to initial conditions with particles that start within a fraction of a laser wavelength following completely different trajectories and gaining markedly different energies.

DOI: 10.1103/PhysRevLett.94.245001 PACS numbers: 52.38.−r, 41.75.Jv, 52.35.−g

The continuing development of high intensity short pulse laser technology has generated much interest in intense laser-plasma interactions. Such interactions produce fast ions, x-rays and relativistic electrons [1]. The acceleration of electrons using laser-plasma interactions has attracted attention due to potential advantages over conventional techniques. In particular, plasmas can support huge electric fields (above 100 GV/m), which are orders of magnitude greater than those in radio frequency accelerators, allowing electron acceleration to high energies in a very short distance [2].

One method for producing large currents of relativistic electrons from laser-plasma interactions has been the self-modulated laser wakefield regime [3–6]. In this regime an intense picosecond laser pulse breaks up into a series of pulselets separated by a distance of $\pi c/\omega_p$. This produces satellites at $\omega_0 \pm n\omega_p$ in the laser spectrum where ω_0 is the laser frequency and $\omega_p = (ne^2/m_e\varepsilon_0)^{1/2}$ is the plasma frequency. The pulselets resonantly drive a relativistic plasma wave until it breaks and accelerates a large current of electrons from the background plasma. In previous experiments with high intensity laser pulses ($I\lambda^2 > 1.5 \times 10^{18}$ W cm^{-2} μm^2) and relatively long pulse lengths ($\sim$1 ps), the acceleration of electrons was strongly correlated with the intensity of Raman satellites in the forward scattered spectrum [3,7–9]. Simulations in that regime confirm that electron acceleration in those experiments was primarily due to the plasma wave generated by the self-modulation instability [10,11].

In this Letter we report that an increase in laser intensity to greater than 10^{20} W cm^{-2} changes the interaction from a regime in which the self-modulated laser wakefield mechanism is dominant to one where a direct laser acceleration mechanism dominates. Simulations show that this mechanism relies on the fact that at early times in the interaction the laser expels virtually all of the electrons in the focal volume creating a cavitated ion channel. A significant fraction of the ions are then pulled out, creating a nearly hollow channel. The space charge field of this channel serves to focus any fast electrons produced in the interaction. At late times when most of the acceleration occurs, the number of accelerated particles increases and the laser begins to diffract, increasing its spot size. As a consequence, the ponderomotive force decreases and the space charge of the accelerated beam expels background electrons, thereby neutralizing its own space charge and leaving only its self-magnetic pinching force. Throughout the interaction, the accelerated electrons feel a net focusing force that confines them within the focal volume. The nonlinear interaction between this focusing force and the laser field allows the electrons to gain significant energy which is converted into momentum in the forward direction due to the $\mathbf{v} \times \mathbf{B}$ force. This energy gain can be many times the ponderomotive potential of the laser, $\frac{1}{2}mc^2a_0^2$ where a_0 is the peak normalized vector potential of the laser field $a_0 = eA_0/mc$.

The experiment reported here was performed using the Vulcan Petawatt Nd:glass laser system, which produced pulses of 160 J in a duration of $\tau = 650$ fs (FWHM). The laser was focused to a 6 μm diameter spot at the edge of a supersonic 2 mm diameter helium gas jet using an $f/3$ off-axis parabolic mirror. This produces peak intensities in

excess of 3×10^{20} W cm^{-2} in vacuum, with a corresponding normalized vector potential of $a_0 \simeq 15$.

To observe the degree of self-modulation of the laser pulse (which can be correlated to the production of plasma waves) a section of the transmitted laser beam was collimated and transported out of the vacuum chamber to an optical spectrometer. To allow the simultaneous measurement of the electron spectrum the section of the beam was slightly off-axis but within the cone of the diverging laser beam.

Raman satellites in the transmitted laser spectrum allow the electron density n_e to be measured. The plasma density is controlled by changing the backing pressure of the gas jet. The electron density observed is close to that expected for the nozzle shape from neutral density measurements.

The energy spectrum of electrons accelerated forward along the axis of laser propagation was measured using a magnetic spectrometer, which had 38 mm diameter pole pieces with a maximum magnetic field of 0.83 T. The entrance of the spectrometer was a collimator with a 5 mm aperture, corresponding to an $f/600$ collection cone. Lead shielding, 10 cm thick, between the interaction chamber and spectrometer, reduced the background signal. A detector array was placed perpendicular to the axis 320 mm away from the center of the magnet. Detectors were placed on either side of the laser axis to measure the electron spectrum below the axis and the background above the axis. The electron energy as a function of deflection was calculated using a 2D particle tracking code that considers the measured shape of the magnetic field and the electron beam divergence. High resolution spectra were taken using Fuji BAS MS-2025 image plates, which produce a 2D image of the dose deposited by electrons passing through the detector plane. The image plates were scanned with 200 μm resolution using a Fuji 1800II image plate reader. The background x rays, generated either in the interaction itself or by the electrons as they pass through material in the chamber, was found to be symmetric above and below the axis, and was subtracted.

In addition, measurements of the electron beam divergence were made by intercepting the whole electron beam with a multilayer stack of radiochromic film (RCF) and copper. The RCF gives a response proportional to dose, and the energy deposited in successive films was deconvolved from the range of electrons in the stack to give a measure of beam size as a function of energy.

Figure 1 shows three electron energy spectra observed at different electron densities, which are representative of the trend observed over the range $n_e = 5 \times 10^{18}$–1.4×10^{20} cm^{-3}. The spectra have large energy spreads typical of laser-plasma interactions, although in this experiment not all the spectra are well described by a quasi-Maxwellian distribution. The spectra with the most energetic electrons were more accurately described by a power law distribution. The spectrum recorded at $n_e = 7.7 \times 10^{18}$ cm^{-3} shows the highest observed electron energies. The signal descends into the background at 300 MeV. The beam divergence measurements show that close to the optimum density the beam divergence was approximately 50 mrad for electrons above 1.5 MeV.

Figure 2(a) shows the transmitted laser spectrum measured simultaneously to the corresponding electron spectra in Fig. 1. The transmitted laser spectra show much lower sideband intensities, by more than a factor of 3, than previous experiments performed at lower intensity with the Vulcan laser [3,7]. In those lower intensity experiments a strong correlation was observed with increasing modulation in the transmitted spectra and the effective temperature of the electron beam.

Figure 2(b) shows that at the higher intensity available in this experiment, the correlation is no longer observed. In fact the highest beam temperatures are observed when the level of modulation is small. Furthermore, the satellites in Fig. 2(a) are broad relative to the fundamental over the range of densities measured. The width of these satellites indicates that plasma waves are being driven to wave breaking at all densities [3]. The lack of correlation between laser pulse modulation and the electron beam effective temperature strongly suggests that the principal mechanism for these parameters is not plasma wave acceleration. The same density dependence for electron acceleration and Raman satellite intensity was observed when the experiment was repeated with deuterium gas as the target.

To investigate the acceleration mechanism a number of 2D (x, y, p_x, p_y, p_z) particle-in-cell simulations have been performed with OSIRIS [12]. The principal conclusions from the simulations are that plasma waves are not the dominant acceleration mechanism, that the majority of fast electrons exhibit stochastic acceleration in the nonlinear focusing field of the ponderomotively driven channel and that the highest energy electrons exhibit betatron-like resonance motion [13,14]. However, it is not possible to predict which electrons will obtain high energy and for the low

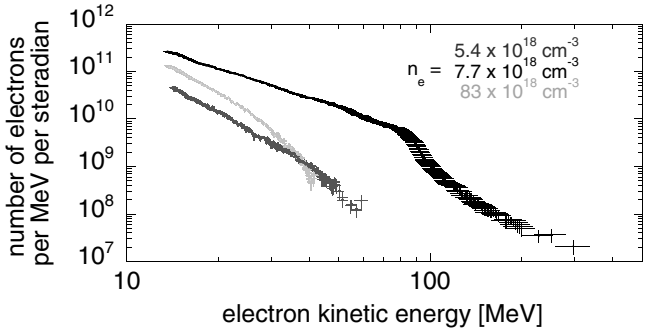

FIG. 1. Three example electron energy spectra observed at various background electron densities for laser intensity $\sim 3 \times 10^{20}$ W cm^{-2}.

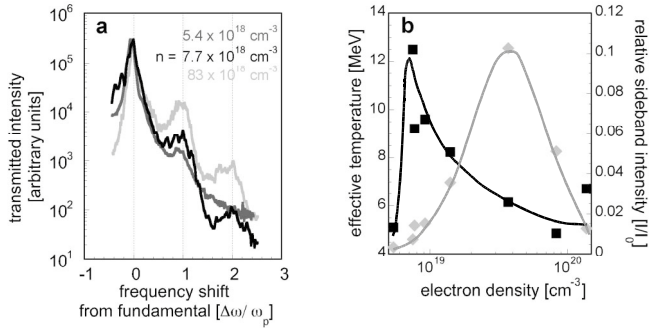

FIG. 2. (a) The transmitted laser spectra corresponding to the electron spectra in Fig. 1. (b) The effective temperature of the electron beam (black squares) and side band amplitude normalized to the signal at ω_0 (gray diamonds) as a function of electron density. The lines in (b) are a visual aid only.

plasma densities considered here a stochastic preacceleration mechanism is needed in order to get into resonance.

The particle-in-cell (PIC) simulations were performed with a high resolution of 40 cells per laser wavelength and the time step was carefully chosen to ensure that numerical dispersion was not a factor. This was confirmed by performing runs where the laser was S-polarized $\mathbf{E} = E\hat{\mathbf{z}}$ and ensuring that transverse canonical momentum a_z-p_z was conserved. In the simulations presented here the laser is P-polarized $\mathbf{E} = E\hat{\mathbf{y}}$ in which case the transverse canonical momentum is affected by forces due to finite laser width and due to the plasma. The plasma profile in the simulations modeled that of the experiment with a 450 μm linear ramp from vacuum to a bulk density of $n = 0.01$ $n_c = 10^{19}$ cm^{-3} for the simulation presented.

In the simulations the laser pulse, which is many times the critical power for self focusing, forms a single self-focused channel containing most of the laser energy. Figure 3(a) shows the laser envelope after the laser has propagated 1.1 mm. In this channel the electrons are virtually completely expelled due to the transverse ponderomotive force. This creates a bare ion channel. On the time scale of the 650 fs laser pulse the ions begin to move radially in the channel due to this space charge field. The expulsion is so strong that an electrostatic shock is formed which propagates outward from the channel leaving a nearly hollow channel behind. Indeed in the experiment helium ions were observed up to 13 MeV [15]. The movement of the ions and the presence of the shock front lead to a highly nonlinear focusing force. As the number of accelerated electrons in the beam increases, so does the space charge and the azimuthal magnetic field associated with it. These self-fields nearly cancel so that the net force is due to the ion channel. However, as the laser propagates down the density gradient it begins to diffract; this lowers the ponderomotive force and now the background electrons respond to the electric force of the beam, thereby space charge neutralizing it. After $\simeq 1.2$ ps the focusing force is therefore dominated by the beam's self-generated magnetic field leading to a nearly harmonic betatron motion. It is at this time that acceleration to the highest energies occurs.

Figure 3(b) shows the channel focusing force $F_y = (E_y - B_z)$. Figure 3(c) shows the p_x-x phase space of the electrons. Clearly showing accelerated electrons beyond 100 MeV throughout the pulse. The electrons are bunched at both twice the laser frequency (not visible on the plot) due to the $\mathbf{v} \times \mathbf{B}$ force and the plasma frequency due to a Raman type instability in the cavitated channel [16]. The bunching is not due to the presence of an accelerating plasma wave but is due to the modulation of the laser envelope only.

In the code we track $\mathbf{p} \cdot \mathbf{E} = \frac{1}{2}\frac{d}{dt}\gamma^2$ for the electrons. This diagnostic shows that longitudinal fields are not responsible for the acceleration. A plot of $\Gamma_y^{1/2} = (\int 2p_y E_y dt)^{1/2}$ against γ [Fig. 3(d)] shows a direct correlation between the energy gained and the work done by the transverse fields (i.e., laser and focusing electric field); the

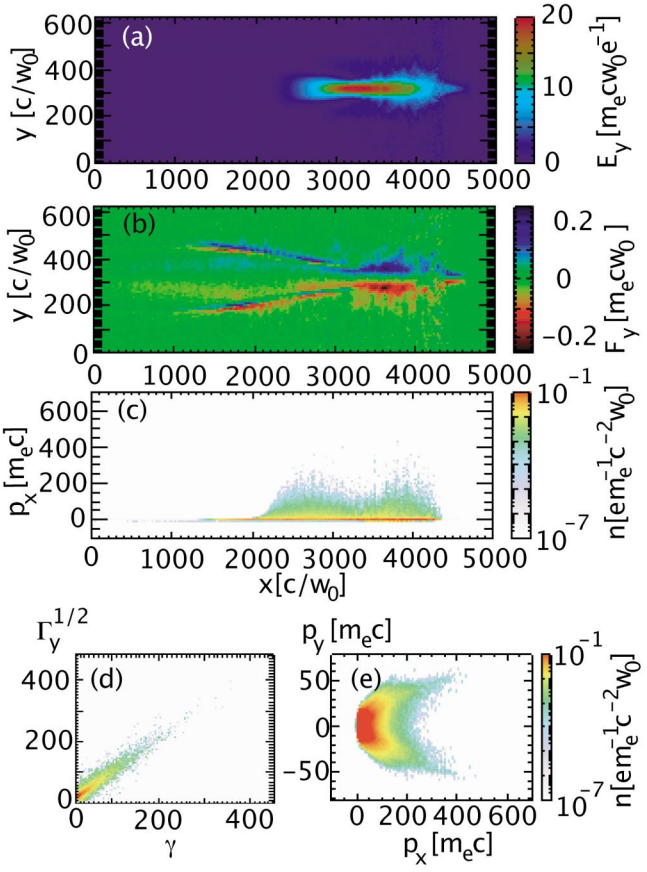

FIG. 3 (color). (a) Laser envelope, (b) channel focusing force, $F_y = E_y - B_z$, (c) p_x-x phase space of electrons, (d) $\Gamma_y^{1/2} = (\int 2p_y E_y dt)^{1/2}$ vs γ of the electrons and (e) p_x-p_y phase space from a simulation at $n = 0.01$ $n_c = 10^{19}$ cm^{-3} after 1.2 ps of propagation.

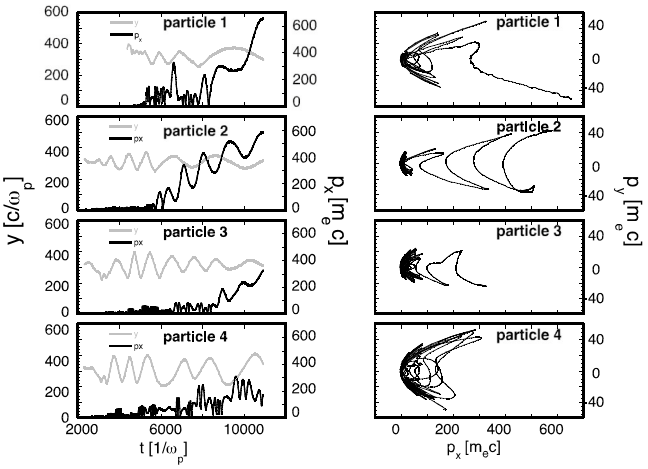

FIG. 4. Trajectories of four typical test particles left column y and p_x vs t, right column p_y-p_x trajectory.

slope of this graph is close to 1 indicating that the energy gained from longitudinal electric fields is negligible. The p_y-p_x [Fig. 3(e)] phase space of the electrons shows a distinct parabolic shape reminiscent of the well known $p_x = \frac{1}{2} p_y^2$ trajectory of an electron in a plane wave. The transverse component extends well beyond the laser's vector potential demonstrating the importance of the transverse field of the channel. The parabola has also been ''filled in,'' indicating a diffusion in phase space corresponding to a stochastic acceleration.

The trajectory and final energy gain of the electrons is strongly dependent on their initial position. Four test particle trajectories, numbered (1–4) are shown in Fig. 4. All particles start at rest and particles 2–4 all start within a fraction of a laser wavelength. All of the particles exhibit oscillations across the channel, but it is clear that this motion is not a simple betatron resonance oscillation.

Particles 1–3 exhibit betatron resonance behavior, with the frequency of the channel oscillation decreasing with the increase in γ. Before the resonant stage, the acceleration is much less regular. The betatron frequency can change abruptly due to the nonlinear nature of the channel restoring force. Particles (e.g., 1–3) which reach the betatron resonance represent a small fraction of the population of fast electrons.

How particles eventually reach a resonance can be complicated. For example, particles 1 and 3 exhibit ''jumps'' in momentum at various points in the simulation before they reach a resonance, indicative of a stochastic preacceleration. Particle 4 is representative of the majority of fast electrons. It experiences nonresonant acceleration due to the combination of the laser and channel fields, the amplitude and frequency of the channel oscillation changes a number of times, resulting in a more complex trajectory.

In most cases where a resonance is reached this occurs when the laser is in the density gradient at the exit of the gas jet. This is due to both the focusing force becoming more linear and laser amplitude becoming more uniform during a betatron excursion due to the increase in the laser spot size.

The nonlinear motion means that the electron trajectories are sensitive to the initial conditions. Small changes lead to dynamics exhibiting betatron resonance, stochastic/diffusive-like motion, or no significant acceleration at all. In particular the preacceleration process necessary to reach the resonant behavior seems to be stochastic in nature.

In our experiment at higher densities propagation instabilities, notably laser hosing and filamentation can occur which significantly degrade the electron acceleration. These have been observed in higher density simulations for these experimental parameters, as well as in previous experiments [17], and are a likely cause of the degraded electron acceleration observed at high density. The electron energies measured in this experiment are the highest yet produced in a laser initiated acceleration mechanism. Furthermore we have observed that increasing the intensity of the laser interaction has changed the acceleration regime from a plasma wave accelerator to one where laser acceleration in an ion channel is dominant. At higher densities the energy at which resonance occurs is lower. Interestingly, the resonant energy is similar to the linear dephasing energy limit for acceleration in plasma waves. A direction for future work is to study whether or not direct laser acceleration can lead to significant energies beyond the betatron resonant energy limit.

The authors would like to thank the staff at the Rutherford-Appleton laboratory for their assistance during the experiment. This work was supported by EPSRC and by DOE under Grants No. DE-FG03-03ER54721, No. FG03-NA0065, No. FG03-02-ER4727, and No. GC02-01ER41179.

*Permanent address: Department of Physics, University of Alberta, Edmonton, Canada

[1] P. A. Norreys, Phys. World **Sep**, 39 (2002).
[2] T. Tajima and J. Dawson, Phys. Rev. Lett. **43**, 267 (1979).
[3] A. Modena *et al.*, Nature (London) **377**, 606 (1995).
[4] M. I. K. Santala *et al.*, Phys. Rev. Lett. **86**, 1227 (2001).
[5] P. Sprangle *et al.*, Appl. Phys. Lett. **53**, 2146 (1988).
[6] R. Wagner *et al.*, Phys. Rev. Lett. **78**, 3125 (1997).
[7] Z. Najmudin *et al.*, Phys. Plasmas **10**, 2071 (2003).
[8] C. A. Coverdale *et al.*, Phys. Rev. Lett. **74**, 4659 (1995).
[9] A. Ting *et al.*, Phys. Plasmas **4**, 1889 (1997).
[10] K. C. Tzeng *et al.*, Phys. Rev. Lett. **79**, 5258 (1997).
[11] D. Gordon *et al.*, Phys. Rev. Lett. **80**, 2133 (1998).
[12] R. A. Fonseca, *Lecture Notes in Computer Science* (Springer, Heidelberg, 2002), Vol. 2329, pp. III–342.
[13] A. Pukhov *et al.*, Phys. Plasmas **6**, 2847 (1999).
[14] C. Gahn *et al.*, Phys. Rev. Lett. **83**, 4772 (1999).
[15] M. S. Wei *et al.*, Phys. Rev. Lett. **93**, 155003 (2004).
[16] G. Shvets and X. Li, Phys. Plasmas **8**, 8 (2001).
[17] Z. Najmudin *et al.*, Phys. Plasmas **10**, 438 (2003).